This manuscript has been submitted for publication in the special issue ***Cave Deposits: Processes, Approaches and Environmental Significance*** in ***Frontiers in Earth Science Quaternary Science, Geomorphology and Paleoenvironment***. This pre-print has **not undergone peer-review** and subsequent versions of the manuscript may differ from this version. If accepted, the final version will be available via a DOI link on this page. Please contact the corresponding author by email with any queries – pennos4@gmail.com Prepared for EarthArxiv on 24th June 2021.

Deciphering late Quaternary climatic histories from the Hermes Cave speleothem record, Corinth Rift, Greece

Pennos Ch.[1,2], *Pechlivanidou S.*[1], *Modestou S.*[1,3,4], *Persoiu A.*[2,5,6], *Ninnemann U.*[1,3], *Gawthorpe R.*[1], *Maccali J.*[1], *Lauritzen S-E.*[1], *Thuesen Th.*[1]

[1] Department of Earth Science, University of Bergen, Bergen, 5020, Norway

[2] Emil Racoviţă Institute of Speleology, Romanian Academy, Cluj-Napoca, 400006, Romania

[3] Bjerknes Centre for Climate Research, Bergen, 5007, Norway

[4] Department of Geography and Environmental Sciences, Northumbria University, Newcastle upon Tyne, NE1 8ST, UK

[5] Stable Isotope Laboratory, Ştefan cel Mare University, Suceava, 720229, Romania

[6] Romanian Institute of Science and Technology, Cluj-Napoca, 400022, Romania

Keywords: speleothem, paleoclimate, Late Quaternary, Corinth Gulf, Eastern Mediterrannean

Abstract

The Greek peninsula is located at the crossroads of several major atmospheric circulation patterns and is consequently characterized by high variability in climatic conditions, making it an important location to examine past climate variability. Over the last decades, the focus of many studies in the region has been to unravel Holocene paleoclimatic oscillations and their impact on the development of ancient civilizations using terrestrial archives and especially speleothem records.

In this study we contribute to the regional climate record over the Quaternary using a speleothem from the Hermes Cave located at the southern flanks of the Corinth Rift in central Greece. Our stalagmite grew over two distinct periods, from ~127 to 105 ka and from 18 to 8 ka B.P. separated by a distinct hiatus. We have examined its growth history, stable isotope geochemistry and elemental composition. Higher growth rates are observed during the Eemian and the early Holocene and are attributed to high water recharge implying humid conditions. A gradual isotopic enrichment before the growth hiatus of the stalagmite suggests a gradual drying that can be related to glacier advance. Our record correlates with other paleoclimate records from the broader area confirming and extending a pattern of coherent changes in paleoclimate across the Eastern Mediterranean basin.

1. Introduction

Climate in the Mediterranean Basin (MB) is a complex result of the conjunction of several atmospheric systems: westerlies from the North Atlantic Ocean, subtropical high-pressure systems originating over North Africa's arid zones, the Siberian High pressure system (SH), the North Atlantic Oscillation (NAO) (Lionello et al. 2006 ; Xoplaki et al., 2000) and the African and Asian Monsoons (Lionello and Galati, 2008). North Atlantic Oscillation in particular strongly impacts winter atmospheric circulation patterns in the MB, with subsequent effects on river runoff (e.g. Tsimplis et al., 2006: Zerefos et al, 2011). Examining climatic patterns over the past 500 years, Luterbacher et al. (2006) concluded that a negative NAO index is related to wet and cool conditions in the MB, while a positive NAO index is associated with strong westerlies at high and mid latitudes, and dry and warm conditions in the MB.

However, the interplay of the atmospheric systems does not have the same intensity across the whole length of the MB. For example Luterbacher and Xoplaki (2003) suggest that there is a clear differentiation between the Eastern Mediterranean basin (EMB) and the Western and Central Mediterranean. Winter air temperature in the Eastern part appears to be negatively correlated with the NAO index, in contrast to the Western and Central part where there seems to be a small positive correlation (Zerefos et al., 2011).

Climate research continues in the MB, utilizing many different archives from the area. Many are based on marine bio-proxies, and aim to understand the paleoceanographic evolution in the EMB and the prevailing paleoclimatic conditions driving that evolution (e.g. Triantaphyllou et al., 2009; Koukousioura et al., 2012; Kouli et al., 2012; Rohling et al., 2015; Triantaphyllou et al., 2015; Gogou et al., 2016; Rohling et al., 2019). Terrestrial records can also provide insight, in some cases more directly, on the paleoclimatic evolution of the area. Existing records are many and diverse, including pollen studies (e.g. (Tzedakis et al., 2002; Tzedakis et al., 2006; Tzedakis, 2010; Jones et al., 2012; Milner et al., 2013), speleothems (e.g. Bar-Matthews et al., 2000; Fleitmann et al., 2009; Psomiadis et al., 2009; Finné et al., 2014; Finné et al., 2015; Nehme et al., 2015; Nehme et al., 2018; Psomiadis et al., 2018; Regattieri et al., 2018; Peckover et al., 2019; Regattieri et al., 2020), geomorphic indexes (e.g. Styllas et al., 2018; Leontaritis et al., 2020) and clastic sedimentary sequences (e.g. Lespez et al., 2017; Styllas and Ghilardi, 2017; Katrantsiotis et al., 2019; McNeill et al., 2019; Pennos et al., 2021). Despite this plethora of publications, most of the studied records do not present a continuous temporal extent for the late Quaternary and/or focus mainly on the time span that ancient civilizations flourished.

Here we aim to investigate the paleoclimatic evolution of the area from a stalagmite collected from the Corinth rift shoulder in southern Greece which covers parts of the late Quaternary and early

Holocene. We compare our results with other speleothem records from the area to understand regional scale climate dynamics, and to compliment the findings of the recent IODP Expedition 381 (McNeill et al., 2019) to decipher climate forcings affecting fluvial sediment fluxes in the Gulf of Corinth.

2. Setting

Hermes cave (HC) is located on Kyllini mountain at 1614 m a.m.s.l. close to Ziria ski resort in the Peloponnese peninsula in southern Greece (Fig.1). It is named after the ancient god Hermes, who, according to Greek mythology, was born and raised inside the cave. The cave entrance is located on a cliff facing towards Flabouritsa valley and the Gulf of Corinth. The cave has been known since antiquity, and has been visited by numerous people throughout the years who caused extensive damage to the speleothems.

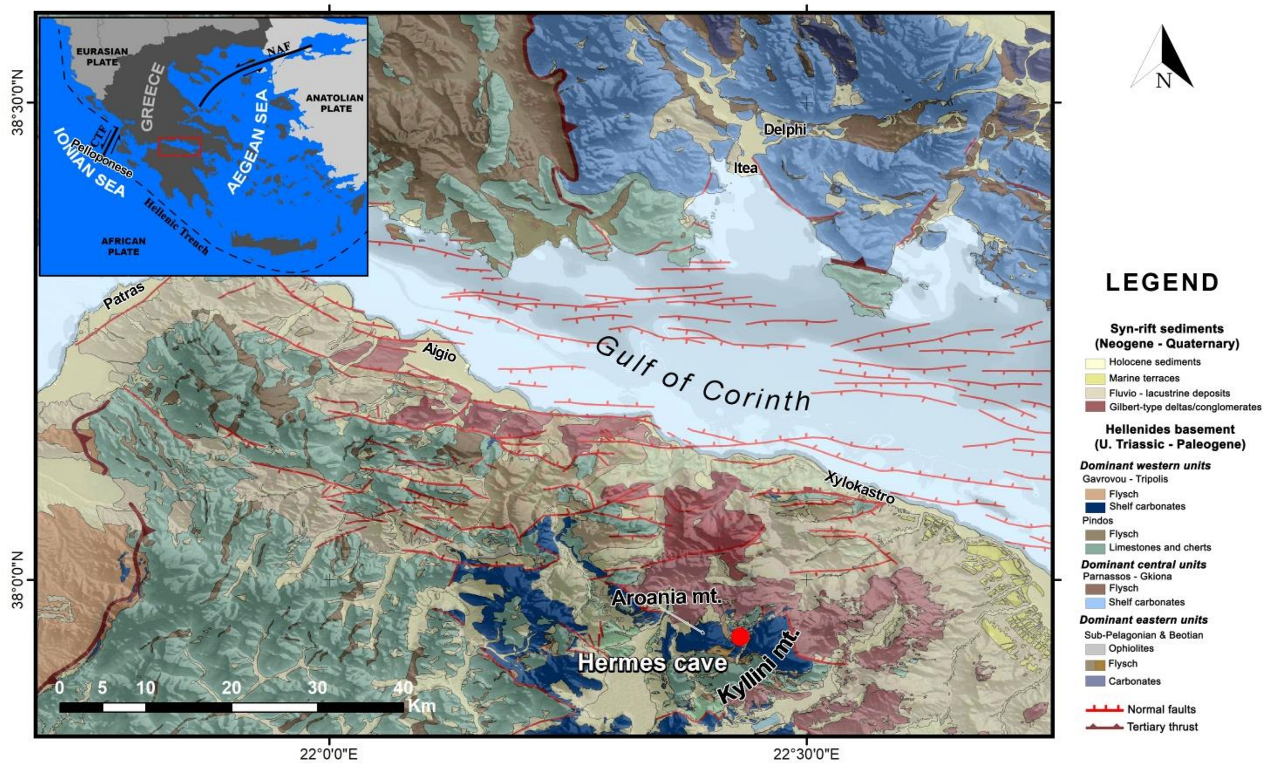

Figure 1. Regional geological map modified from Skourtsos et al. (2017).

It formed in upper Triassic-Paleogene limestones belonging to the Gavrovo-Tripoli geotectonic zone of the Hellenides orogenic belt (e.g. Skourtsos et al.,2017; Gawthorpe et al., 2018). These carbonates outcrop on the southern flank of the Corinth extensional rift, and have undergone brittle deformation and are densely fractured. The extensive fracturing allowed surface water to penetrate into the limestone and initiate cave formation. Hermes Cave is elongated in a NE-SW direction and the cave floor dips steeply, >45°, toward the SW, following the bedding of the limestones. Speleothem formations are extensive, with stalagmites intercepting rock debris and forming small terraces in some places.

The modern climate in the broader area corresponds to "Mediterranean Climate" with 9.7^{o}C mean annual temperature and 1296 mm mean annual precipitation (Mamara et al., 2017). The climate is characterized by mild and wet winters (December – March) that contribute most of the annual precipitation, with dry, warm summers where occasional convective precipitation occurs, resulting in strong, stormy rainfall events (Xoplaki et al., 2000; Feidas et al., 2007). Xoplaki et al. (2004) concluded that although there is large spatio-temporal variability in the region's winter precipitation, a significant portion (30%) is explained by large-scale atmospheric circulation. This pattern is clearly observed when winter NAO-driven depressions move north east from the North Atlantic through the Gibraltar straits and release rainfall on western Greece (Styllas et al., 2015 and references therein).

3. Methods

3.1 Speleothem sampling

In order to collect a stalagmite that is active throughout the year and records both winter and summer precipitation, we visited the cave during the dry season (late August). We collected an active stalagmite (ZCG1) in situ from a relatively small chamber far from the entrance (Fig.2), where no air draft was evident, to exclude any drip water evaporation. The sampling chamber is a small blind passage, 6 m long, 2.5 m high and 4 m wide, that dips steeply towards the main development axis of the cave. It is located 50 m from the entrance and ca 60 m below the surface. The 30 cm tall stalagmite was extracted from the cave and was later cut in half along the growth axis. One part of the stalagmite was stored for reference, and from the other half a 2 cm thick slab was extracted. From macroscopic observation it is evident that ZCG1 is a densely laminated stalagmite. Most of the laminae are opaque, with no visible signs of diagenesis of the calcite fabric (Fig. 3).

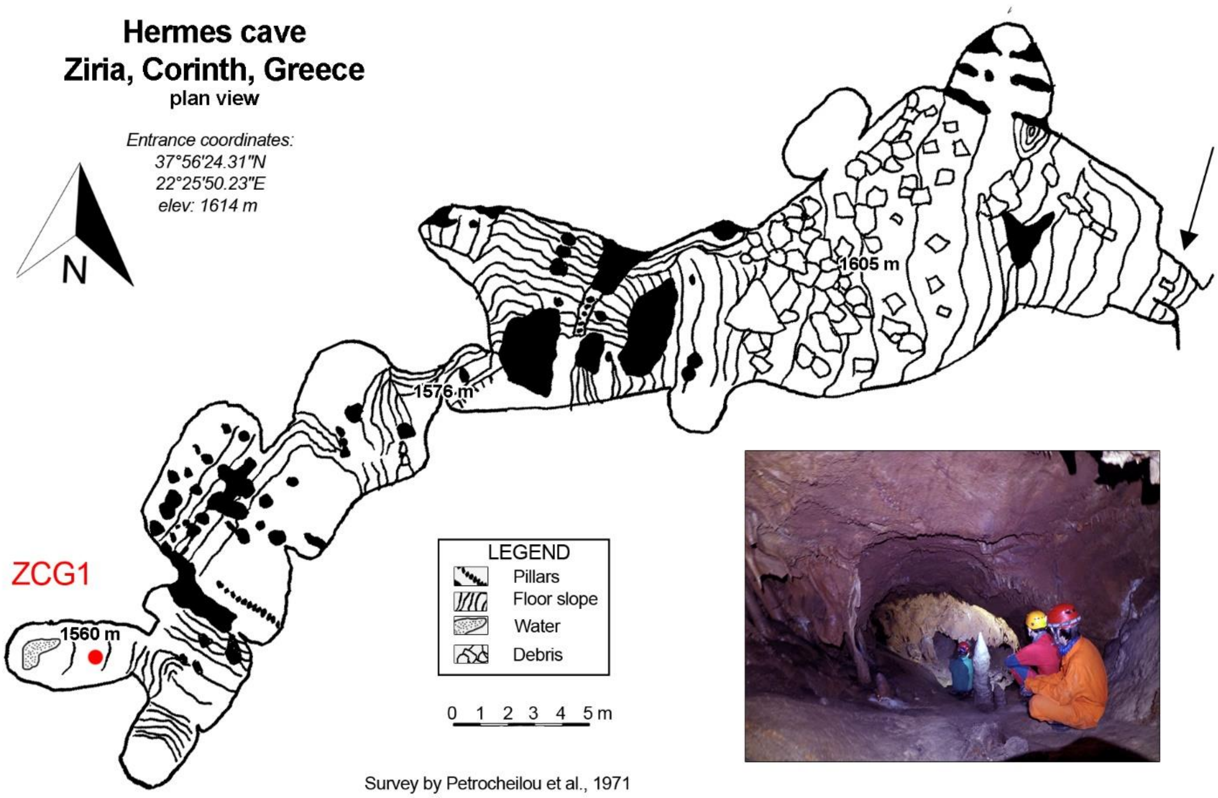

Figure 2. Plan view of Hermes Cave from Petrocheilou (1972). Red dot shows the position of the stalagmite. Inset photograph shows the chamber where stalagmite ZCG1 was formed.

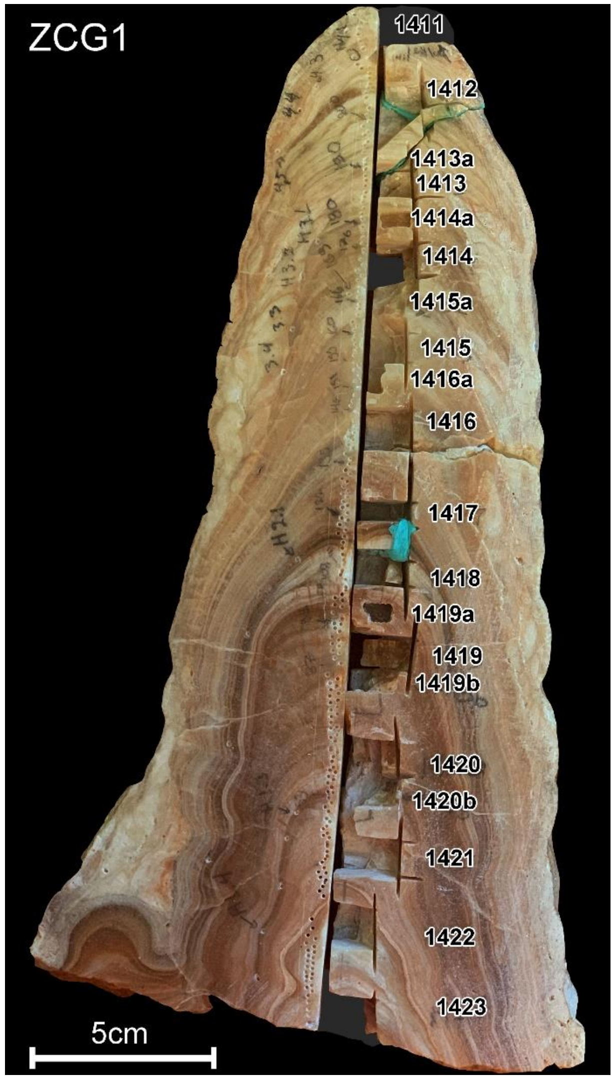

Figure 3. Polished section of the ZCG1 stalagmite. Small pits indicate stable isotope sampling position. Rectangular trenches indicate the position of the Th/U samples with their corresponding lab id.

3.2 Th/U dating

To construct the age-depth model, we extracted seventeen samples along the growth axis either by drilling or milling. Samples were first heated at 650°C for 4 hours to remove organic material.

Chemical separation of U and Th was adapted from Edwards (1988). The samples were spiked with a mixed ^{233}U-^{236}U-^{229}Th solution (calibrated against Harwell Uraninite (HU-1) solution considered at secular equilibrium) and dissolved in concentrated HNO_3. Column chemistry cleaned Fe solution was added, and Fe precipitates were formed by dropwise addition of NH_4OH. Fe precipitates were rinsed with 18.2 MΩ deionized water, re-dissolved with 6 M HCl and loaded onto AG1X8 resin for U-Th separation. Uranium and Th were further purified through consecutive passes onto U/TEVA and AG1X8 resins, respectively. Th and U isotopes were analyzed on a Nu Plasma II MC-ICP-MS. Mass bias was corrected by standard-sample bracketing using HU-1 solution. Blank concentrations were $^{238}U < 0.2$ ng; $^{234}U < 30$ fg; $^{232}Th < 11$ pg; ^{230}Th was below the detection limit. Activity ratios were calculated using decay constant values from Bourdon et al. (2003). Ages were calculated using Isoplot 3.75 (Ludwig, 2003) without decay constant uncertainties. Long term analytical reproducibility of the HU-1 solution (n = 28, measured over 15 months) is AR($^{234}U/^{238}U$) 1.002 +/- 0.001 and AR($^{230}Th/^{238}U$) 1.003 +/- 0.002 (2 SD). All U-series data reported in tables are presented with $\pm 2\sigma$ uncertainty, propagated to include analytical and spike calibration uncertainties, unless otherwise indicated.

3.3 Stable isotopes

Stable isotope sampling was performed by milling with a 0.7 mm diameter bit along the growth axis, with 1 mm step, resulting in a total of 218 samples. $\delta^{18}O$ and $\delta^{13}C$ analyses were conducted at the University of Bergen (FARLAB) using a MAT 253 mass spectrometer coupled to an automated Kiel IV preparation device. Approximately 50 (±20) µg of sample powder was reacted with concentrated ortho-phosphoric acid (H_3PO_4) at a constant 70 °C. Isotope values are reported on the Vienna Pee Dee Belemnite (VPDB) scale calibrated using the scale reference standard NBS

19 (value 1.95‰ and 2.2‰ for $\delta^{13}C$ and $\delta^{18}O$, respectively) together with NBS 18 (-5.01‰ and -23.2‰ for $\delta^{13}C$ and $\delta^{18}O$, respectively ; Friendman et al.,1982; Hut, 1987; Stiltcher,1993; Coplen et al., 2006 refs) . Analytical reproducibility (1s), based on replicate measurements of the in-house carrara marble standard CM12 spanning the same mass range and run over the analysis period (n=128) was 0.06 and 0.03 $\delta^{18}O$ and $\delta^{13}C$, respectively. Finally, we performed Hendy's tests (Hendy, 1971) within 4 distinct laminae as a first check for correlation between $\delta^{18}O$ and $\delta^{13}C$, providing information about possible kinetic effects during precipitation.

3.4 μ-XRF

Relative elemental composition was determined by x-ray fluorescence using an Itrax core scanner. Core scanning was conducted on the 2 cm thick stalagmite slab, along the growth axis at 1 mm intervals using a Mo x-ray tube (Croudace et al., 2006). Exposure time was 10 s, power supply was 30 kV/55 mA. The output was later processed using Q-spec software. Following the calcite growth modelling approach of Wong et al. (2011), we interpret high Sr/Ca values as representing summer season speleothem growth and low values as winter growth, respectively.

4. Results

4.1 Age Model and growth rate

The Th/U analysis produced ages ranging from 7.0 ± 4.2 ka to 127.9 ± 52.5 ka B.P. (Table 1). To generate a growth model we used the Mod-Age software (Hercman and Pawlak, 2012) that employs a weighted scatterplot smoothing (LOESS) interpolation to build the chronological model. Three Th/U dates were indicated by the software to be outliers (see fig4b) and were not used for the model. The growth period covers the period 133.2 to 7.4 ka B.P., but is interrupted by a hiatus in growth at ca 135 mm from the base. This hiatus extends between approximately 105 to 23 ka B.P. (fig.4a).

Table 1. Activity ratios and age calculations from ZCG1 stalagmite.

Sample ID	Depth (mm)	238U µg/g	2σe	(230Th/238U)	2σe	(234U/238U)	2σe	Age uncr (ka)	2σe	(232Th/238U)	2σe	230Th/232Th	2σe	Age cr (ka)	2σe (ka)
1411	0.85	222	7	0.0683	0.0338	1.078	0.074	7.1	4.2	0.0040	0.0020	17.2	8.5	7.0	4.2
1412	2.6	197	7	0.0727	0.0451	1.099	0.093	7.4	5.5	0.0053	0.0033	13.7	8.5	7.3	5.5
1413a*	3.6	197	1	0.0818	0.0005	1.079	0.006	8.6	0.1	0.0042	0.0003	19.6	0.1	8.5	0.3
1413	5.1	196	7	0.0841	0.0352	1.103	0.078	8.6	4.4	0.0078	0.0034	10.8	4.5	8.4	4.4
1414a*	6.15	219	1	0.0866	0.0004	1.109	0.005	8.8	0.1	0.0037	0.0003	23.1	0.1	8.7	0.3
1414	7.2	219	7	0.0789	0.0222	1.095	0.064	8.1	2.9	0.0056	0.0017	14.1	4.0	8.0	2.9
1415a*	8.25	229	1	0.2021	0.0012	1.095	0.006	22.1	0.2	0.0172	0.0035	11.7	0.1	21.9	0.6
1415	9.7	186	6	0.0795	0.0447	1.109	0.078	8.1	5.4	0.0040	0.0023	20.1	11.3	8.0	5.4
1416a*	10.5	344	1	0.0702	0.0004	1.112	0.006	7.1	0.1	0.0023	0.0002	30.4	0.2	7.0	0.2
1416	11.95	176	6	0.1033	0.0431	1.123	0.094	10.5	5.6	0.0190	0.0084	5.4	2.3	10.0	5.5
1417	14.15	165	8	0.2129	0.0688	1.125	0.118	22.7	11.2	0.0915	0.0392	2.3	0.8	20.4	11.0
1418	15.65	77	8	0.7299	0.1407	1.154	0.183	105.6	97.0	0.0813	0.0723	9.0	1.6	103.6	96.6
1419a*	16.85	117	0	0.7040	0.0040	1.125	0.007	104.1	1.5	0.0694	0.0492	10.1	0.1	102.8	5.8
1419	17.95	107	5	0.7381	0.1202	1.101	0.096	117.7	65.8	0.1053	0.0924	7.0	1.3	115.1	65.6
1419b*	18.7	126	1	0.7063	0.0045	1.112	0.007	107.0	1.7	0.0505	0.0359	14.0	0.1	107.9	5.0
1420b*	21.75	158	1	0.7541	0.0043	1.140	0.006	114.1	1.7	0.0972	0.0737	7.8	0.0	114.1	5.4
1423	27.85	243	8	0.7381	0.0879	1.057	0.067	128.3	52.5	0.0151	0.0126	48.7	5.9	127.9	52.5

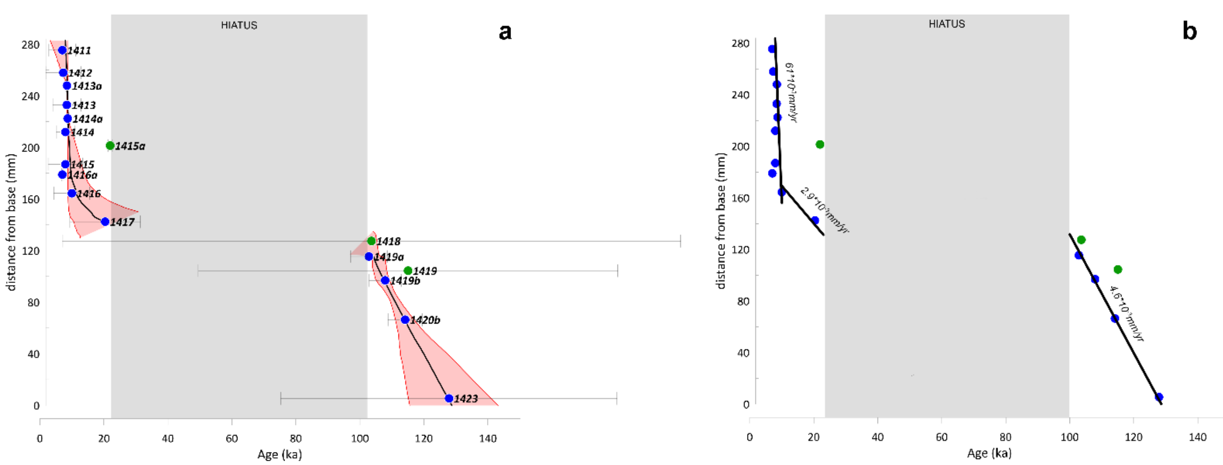

Figure 4. a) Age depth model. Blue dots are dating results, horizontal error bars are 2σ. Red shading illustrates the 2σ uncertainy of the age model. Outliers are shown in green. b) Growth rates of the stalgmite indicated per major intervals.

To estimate the growth rate for each interval, we employed a linear regression approach. Three different linear regression lines with high coefficient (R^2 > 0.85) were generated (Fig.4b). The oldest part of the stalagmite developed between 127.9 ka to ca 105 ka B.P. at a rate of 4.6 x 10^{-3} mm/yr. Following the growth hiatus the rate between 20.4 ka to 10 ka B.P was lower at 2.9 x 10^{-3} mm/yr. but the youngest part of the stalagmite, 10 ka to 7 ka B.P., formed at a much higher growth rate of 6.1 x 10^{-3} mm/yr (Fig.4b).

The age estimate for the oldest sample (1423, Table 1, Fig. 3) has relatively poor precision. This age estimate is critical for constraining the age model as it lies at an end point, thus the measurement was repeated with a new portion of stalagmite material. Unfortunately, the result of this repeat measurement were not improved over the original, likely due to detrital contamination. To compensate for the resulting age model uncertainty on ages older than ~ 115 ka, we compare the stable isotope results grouped over the Last Interglacial (116 – 129 ka; Tzedakis et al., 2018) and Holocene (to ~12.5 ka; Styllas et al., 2018) according to the median age model dates, and compare to the same data but given ages at the maximum and minimum values of the age model error envelope (see discussion).

4.2 $\delta^{18}O$ and $\delta^{13}C$ record

The results from the Hendy tests (Hendy, 1971) suggest isotopic equilibrium conditions during the majority of ZCG1 deposition (see suplementary). It is evident that the variations of $\delta^{18}O$ and $\delta^{13}C$ show no positive correlation along each of the tested layer, and there is no enrichment in ^{18}O towards the external part of the stalagmite. The exception to this is near the termination of growth before the hiatus, which is marked by an isotopic enrichment (Fig. 5) that might be indicative of kinetic effects, possibly due to a change in climatic conditions.

$\delta^{18}O$ values range from -8.8 to -6.2 ‰ (Fig. 5). For the first 10 ka of stalagmite development the values show minor variations from -7.7 to -6.7 ‰ until ca 123 ka B.P. This period is followed by a period of lower values (down to -8.7 ‰) lasting for almost 3000 yrs. An increase in $\delta^{18}O$ values follows, which peaks at 118 ka B.P (maxima -6.8 ‰). This period is trailed by a decrease of $\delta^{18}O$ values until ca 115 ka B.P. where the values osciliate between -7.9 and -7.3 ‰ up until 112 ka B.P. From 106 ka B.P. to ca105 ka B.P. when the growth of the stalagmite is halted, δ18O values grow again (maxima -6.2 ‰) but, as stated above, this might be indicative of kinetic effects thus will not be interpreted in terms of climate.

At ca 20 ka B.P. the stalagmite resume growth and the δ18O exhibits a slight increase, from -8.3 to -7.9 ‰, for the succeeding 3.5 ka. This period is followed by an abrupt decrease in δ18O to -8.5 ‰, followed by an interval of minor osciliations (between -8.5 to -8 ‰) until ca 11 ka B.P. Low values of $\delta^{18}O$ are recorded during the next growth interval until ca 10.7 ± 3.5 ka B.P., followed by a general increase in δ18O to -7.4 ‰ that peaks at ca 8.5 ka B.P. This increase of the $\delta^{18}O$ values is interrupted by two prominent negative peaks at 9.5 ± 3 and 9.1 ± 3 ka B.P. ($\delta^{18}O$ values -8.72 and -8.7 ‰ respectively). Finaly, at the youngest part of the stalagmite after a sharp decrease, $\delta^{18}O$ values oscilliate from -8.4 to -7.8 ‰ when the stalagmite growth halts at ca 8 ka B.P.

$\delta^{13}C$ values range between -10.4 to -3.5 ‰ VPDB (Fig.5). From 126 ka to 115 ka B.P., $\delta^{13}C$ show slight variations from -8.7 to -8.2 ‰. After a short and sharp ^{13}C enrichment at 113 ka B.P., a period of ca 4 millenia with minor osciliations in $\delta^{13}C$ values follows. During the next evolutionary stage of the stalagmite, a strong increase in $\delta^{13}C$, around -3.7 ‰, , and lasts for ca 2 millenia. Different growth conditions, starting at A new period begings with a sharp decrease of $\delta^{13}C$ at ca 111 ka BP, continuing with slight variations overprinted on this long term ^{13}C-depletion until the stalagmite growth is interrupted at ca 105 ka B.P. Past the growth hiatus, the $\delta^{13}C$ record presents a slight increase for the succeeding 3.5 ka from -7.5 to -6.5 ‰. From 15.9 to 11.2 ka B.P., $\delta^{13}C$ decreases from -7.6 to -9.7 ‰. At the youngest part of the stalagmite the δ13C values are marginally decreasing, with minor flactuations on the general trend interrupted by four prominent peaks at 10.5, 10, 8.9 and 8.4 ka B.P.

4.3 *μ*-XRF

The XRF measurements generated a detailed trace element profile of the stalagmite. The x-ray fluoresence signal in such dense material as speleothems is strong; consequently, the scan returned good counting results for numerous elements (e.g. Al, Si, P, Sr, Ti, Fe). Here we focus mainly on the Sr/Ca ratio since it can be used as paleoclimate proxy (e.g. (Kluge et al.; Fairchild and Treble, 2009; Wong et al., 2011; Fairchild and Baker, 2012). Six distinct intervals exhibit an excess in Sr compared to Ca at 122, 120-117, 114, 113, 108-106.5. and ca 105 to 104 ka B.P. (Fig.5). After the depositional hiatus and up until 11 ka BP, The Sr/Ca ratios shows minor fluctuations. From 11 ka until ca 9.8 ka B.P. there are two intervals where again an excess in Sr is observed (at 11 and 9.8 respectively). From 9.8 ka B.P. until the end of the record there is general increase on in the Sr/Ca ratio with four peaks at 9.5, 9.1, 8.5 and 8.1 ka B.P.

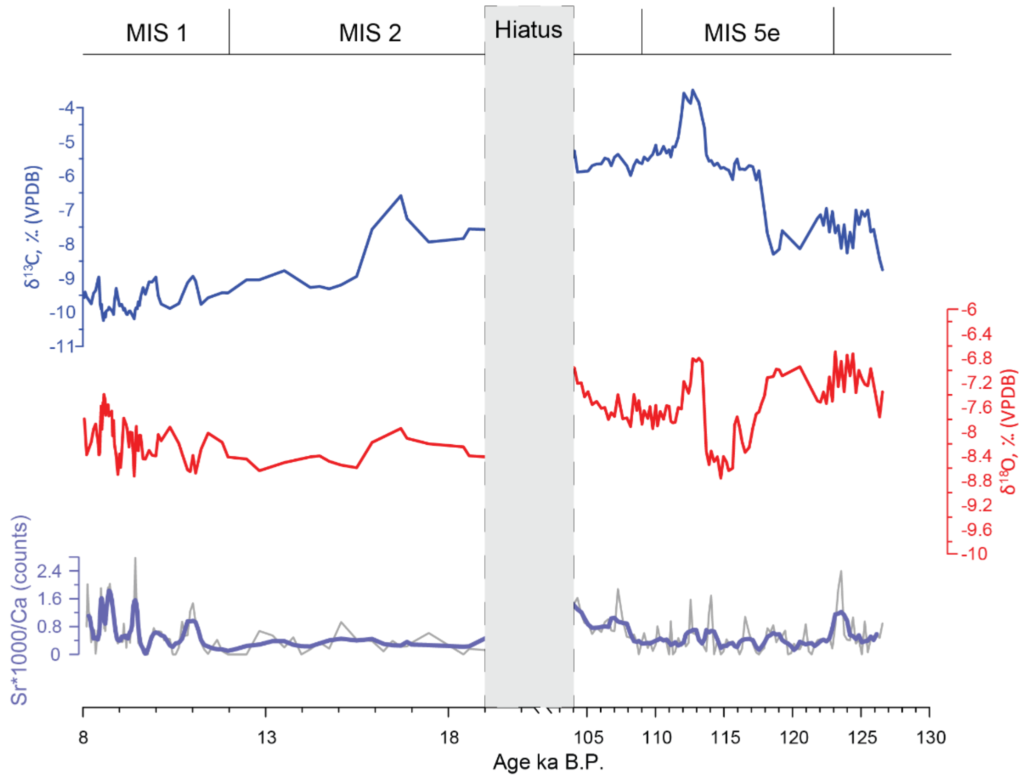

Figure 5. Carbon isotope (blue line), oxygen isotope (red line) and Sr/Ca μ-XRF (black and purple lines) profiles along ZCG1 stalagmite.

5. Discussion

5.1 Major climate patterns

The ZCG1 stalagmite formation started at around 127 ka indicating the establishment of climatic conditions that favored the speleothem deposition in this karstic setting. This period correlates with the beginning of the maximum interglacial conditions that enabled high growth rates recorded in stalagmites across Europe (Drysdale et al., 2009; Genty et al., 2013; Demeny et al., 2017). The carbon isotope signal from the ZCG1 stalagmite reflects soil activity, which itself is dependent on temperature and precipitation regime (e.g. Genty et al., 2001) while the oxygen isotope compositions reflect the combined effect of temperature and moisture source (e.g. Dansgaard, 1964; McDemortt, 2004; Nehme et al.,2015 and references within).

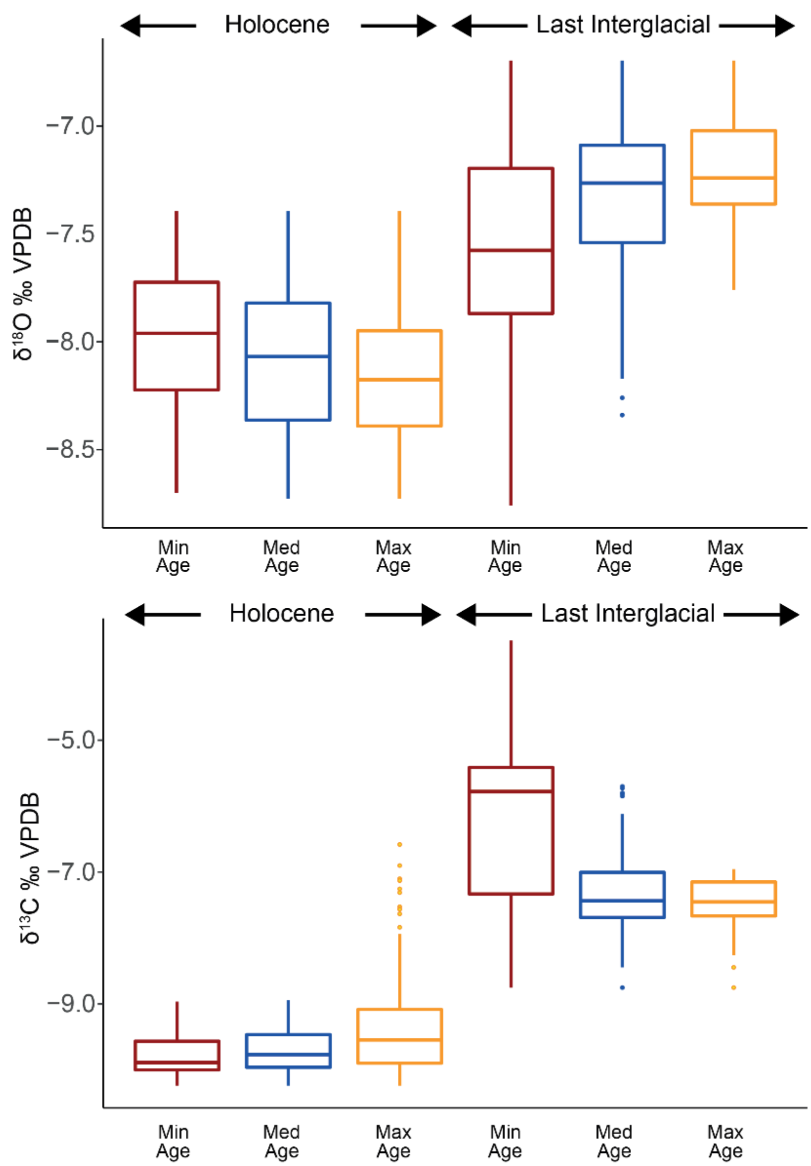

Figure 6. Box plots comparing Ziria speleothem stable isotope compositions from the Holocene (to 11.7 ka) against the Last Interglacial (127 to 116 ka) by possible ages (med age = median age; min age = minimum age at error envelope limit; max age = maximum age at error envelope limit).

Figure 6 compares the stable isotope data from the Holocene (to 11.7 ka) with those from the Last Interglacial (116 to 127 ka), with the data grouped based on different options in the age model (median age, minimum age according to the error envelope, maximum age according to the error envelope). The purpose of this comparison is to examine how the relationship between the overall speleothem isotope composition for each period changes with age. With the exception of $\delta^{18}O$ compositions using minimum age values, all versions of the data are significantly different and show similar differences in isotopic composition. This indicates that, at minimum, the different age possibilities for the oldest part of Ziria stalagmite do not affect broad interpretations of climate for the Last Interglacial period, where the age model has the largest uncertainty. Concurrenly, this shows a higher climatic variability during the Last Interglacial compared to the Holocene as was previously shown by Tzedakis et al. (2018)

Alongside the onset of stalagmite growth, $\delta^{13}C$ values are increasing and the $\delta^{18}O$ values decreasing (Fig. 7), suggesting that at the beginning of the interglacial cycle the climate was colder and drier in the region and had not yet reached stable interglacial conditions (Tzedakis.et al., 2018). Following this period of instability and up to 117 ka, $\delta^{13}C$ values exhibit two minima (at 122 and 117 ka respectively) suggesting high soil activity that can be attributed to forest expansion due to humid conditions that correlate broadly with the growth of near sea level microbial brackish water bioherms(~116 ka) at the Perachora pennnsula, eastern part of the Gulf of Corinth (Portman et al., 2005) due to high influx of fresh water whereas the period between these two excursions exhibits high values that corresponds to a dryer period for the broader area. This is in contrast to Central Europe stalagmite records (e.g., Baradla cave; Demeny et al., 2017; Fig. 7) which indicate this period is considered the optimum within the interglacial (Govin et al., 2015) with high soil activity.

The $\delta^{18}O$ record for the same period exhibits low variation suggesting no major changes in the source or amount of precipitation. The $\delta^{18}O$ values reach a minimum at 115 ka, while concurrently the $\delta^{13}C$ values increase, pointing to low soil productivity and establishment of cold and dry conditions in the area towards the onset of the glacial period. The same trend for both $\delta^{13}C$ and $\delta^{18}O$ values continues until circa 112 ka with an interruption towards 114 ka where the oxygen record exhibits a positive peak and the carbon record a negative peak. We suggest that these changes in the overall trend can be attributed to a period where cyclonic depressions forming over Africa are controlling the climate probably the same ones responsible for the transport of Saharan dust to the area (e.g. Stuut et al., 2009; Philandras et al., 2011; Remoundaki et al., 2011). The reduction in soil activity during this period is most likely related to a change in vegetation, similar to that which occurred in the Balkan peninsula when low vegetation replaced thick interglacial forests (Tzedakis et al., 2004). This change in the type of vegetation slightly enhanced soil activity that resulted in the negative peak on the $\delta^{13}C$ values at around 112 ka. Finally, the growth of the stalagmite continues up to 105 ka until the hiatus, albeit with slightly lower $\delta^{13}C$ values (relative to the 112 ka peak), suggesting that the are is still experiencing a period with low soil activity. The $\delta^{18}O$ record during this growth interval up to the growth hiatus shows low variability and is similar to other records from central Europe (Kern et al., 2019).

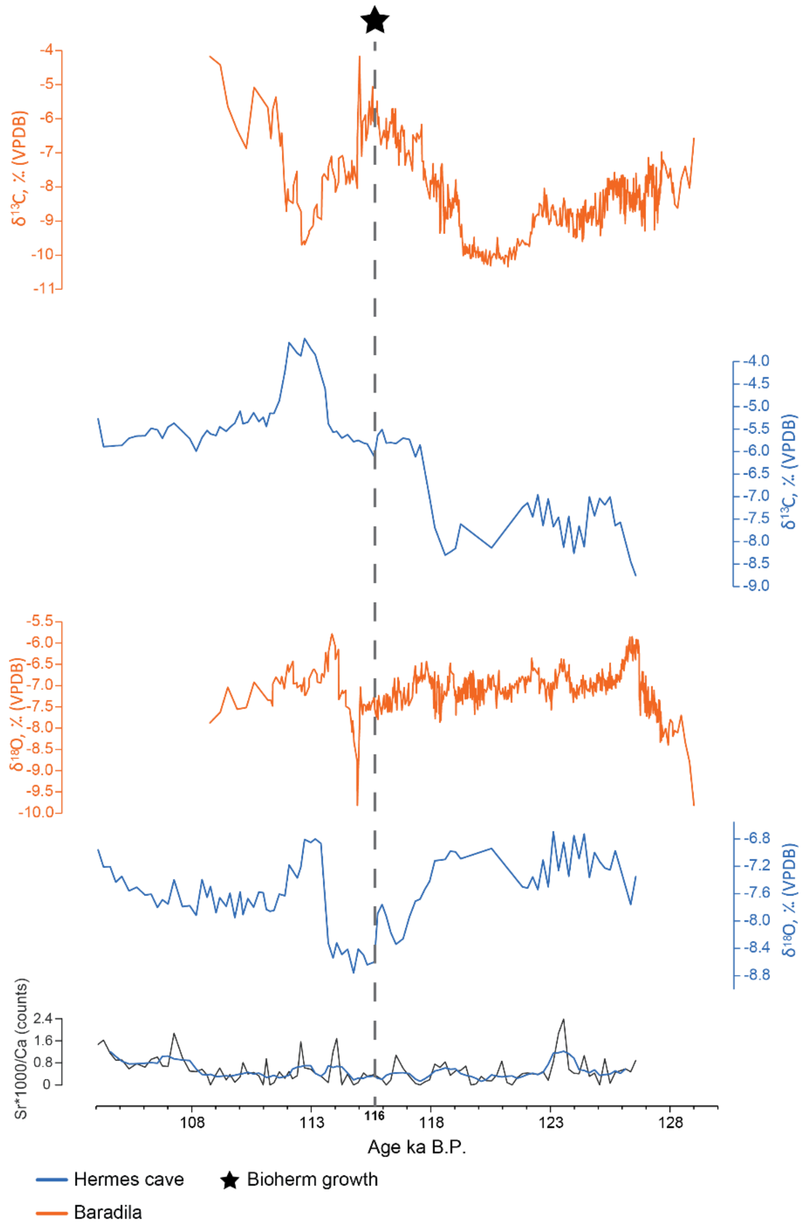

Figure 7. Comparison of ZCG1 last interglacial part with Baradla cave record (Demeny et al., 2017) and bioherm growth (Portman et al., 2005).

Although the stalagmite growth hiatus might have occurred for different reasons we suggest that this was the result of low amounts of water infiltrating into the cave and can be attributed to the existence of small glaciers that occurred in the area and their expansion during the glacial period (Leontaritis et al., 2020). As warm and humid conditions are generally viewed as prerequisites for speleothem growth (Dreybrodt, 1988; Baker and Smart, 1995; Genty et al., 2006; Nehme et al., 2020), inferences about climate can potentially be made from the prescence of speleothem growth hiatuses. Speleothem growth interruptions may also be due to a change in the fluid pathways reaching the cave; while this cannot be ruled out, the fact that ZCG1 recovered and grew throughout the Holocene makes this option less likely. The ZCG1 hiatus (~ 105 to 23 ka B.P; Fig. 3) spans approximately MIS4 to the LGM. MIS3 and MIS4 are thought to generally have been wetter and colder in the Eastern Mediterranean (Bar-Matthews et al., 2003, 2019), indicating conditions more suited to the development of alpine glaciers compared to the warmer temperatures of the preceeding climate phases. In particular, the Eemian (MIS5e) is estimated at 9 – 11°C warmer in the east Mediterranean (e.g. Nehme et al., 2020); temperatures this much higher which would have driven the snowline to a much higher altitude compared to the cooler conditions of later glacial/interglacial cycles. These conditions may have extended to the LGM (Styllas et al., 2015; 2018; Leontaritis et al., 2020 and references within), until at the LGM termination, the temperature and precipitation regime no longer fulfilled the requirements for glacier preservation. After local glaciers either shrank or disappeared, water was able to once again infiltrate Hermes Cave and ZCG1 growth continued. Glacial deposits from the nearby Mount Chelmos have erratics with emplacement dated throughout MIS 3 and the LGM (Leontaritis et al., 2020).

The post-LGM part of the ZCG1 covers the interval from 18 to 8 ka. Our record exhibits higher temporal resolution towards the onset of the Holocene as a result of higher growth rate that is most likely related the increased soil productivity under a warm and wet climate. The $\delta^{18}O$ record exhibits low variability between 18 and 11 ka, after which the values become highly variable on an overall increasing trend linked to the increase in air temperatures and/or humidity after the onset of the Holocene.

The overall trend of the $\delta^{13}C$ records follows that of similar records from regions with comparable climatic conditions - Turkey (Sofular Cave, Fleitmann et al., 2009) and Lebanon (Jeita Cave, Cheng et al. 2015). In all these records including the ZCG1 stalagmite, $\delta^{13}C$ values peak at around 17 ka and drop between 14.7 and 11.3 ka, resuming an increasing trend after the onset of the Holocene (11.7 ka). Similar to the Jeita record, the Bølling-Allerød (BA) and Younger Dryas (YD) are poorly differentiated in the $\delta^{13}C$ record, possibly indicating that different process resulted in similarly low $\delta^{13}C$: enhanced soil productivity linked to post-glacial forest expansion during the warm BA (Feurdean et al., 2014) and increased precipitation delivered by strengthened westerlies linked to the southward displacement of the polar front during the YD (Lane et al., 2013). It is conceivable that while these moisture tracks reached both Greece and the Levant , possibly also picking up moisture from the Eastern Mediterranean, they did not reach the Black Sea coast in Turkey, thus leading to drier conditions there (as indicated by the high $\delta^{13}C$ values during the YD in the Sofular record (Fleitmann et al., 2009). Similarly high $\delta^{13}C$ values were recorded in speleothem P10 in SW Romania (Constantin et al., 2010) at the end of the YD, suggesting dry conditions. Collectively, these observations point towards an important differentiation of climatic conditions between SE Europe and the Eastern Mediterranean region during the YD, with a band of cold and dry climatic conditions stretching from Central Europe across the northernmost Balkan Peninsula towards the northern coast of Turkey, and somewhat wetter conditions in southern Greece and Levant, likely brought about by moisture delivered by southerly displaced westerlies.

The onset of the Holocene is marked by increased variability in the $\delta^{13}C$ and $\delta^{18}O$ records, similar to those seen in the Jeita and Sofular records. In Hermes Cave, several warm (recorded by the $\delta^{18}O$) and wet (recorded by the $\delta^{13}C$) periods punctuate the early Holocene, broadly centered at 9.5, 9.1 and 8.5 ka BP (Fig. 8) and their timing correlates within error with a wet period recorded on the alluvial fans formations in Perachora penninsula (Peckover et al., 2019). These warm peaks are coincident with cooling events in the Carpathian Mts, as recorded by the $\delta^{18}O$ of cave ice (Perșoiu et al., 2017). These cooling periods both in South Greece and in Romania are coincident with high K^+ values measured in the GISP2 record (Mayewski et al., 1997; 2004), which indicate a stronger than usual Siberian High. The Siberian High is a semipermanent high-pressure cell located over Eurasia which affects European and Asian climate in winter (Cohen et al., 2001). Strengthening of the Siberian High results in atmospheric blocking that leads to cold air advection towards northern and central Europe, warming southern Europe and the Levant with stronger than usual clockwise winds across SE Europe and enhanced cyclogenesis over the Central Mediterranean (Perșoiu et al., 2019). These conditions result in increased precipitation delivered to mainland Greece leading to wet conditions and thus potentially explaining the excursions towards negative $\delta^{13}C$ excursions in the ZCG1 speleothem. Alternatively, the increase in anticyclonic winds could have increased the fraction of moisture sourced from the Aegean Sea. Thus, the high $\delta^{18}O$ values of speleothem calcite may have been the result of picked-up moisture from the warmed-up Aegean Sea (e.g. Marino et al., 2009). Speleothem $\delta^{18}O$ records from Peloponnese show contrasting response to changes in precipitation, with the Kapsia record (Finné et al., 2014) indicating high $\delta^{18}O$ values associated with dry conditions while the Alepotrypa record (Boyd, 2015) suggest high $\delta^{18}O$ values are indicators of wet conditions (similar to ZCG1) likely, local infiltration conditions may have an outsized effect on the $\delta^{18}O$-climate relationship. Winter climatic conditions in the early Holocene were possibly under the influence of the predominantly negative phase of the NAO (Perșoiu et al., 2017) resulting in weakened westerly circulation that probably allowed the westward expansion of easterly winds.

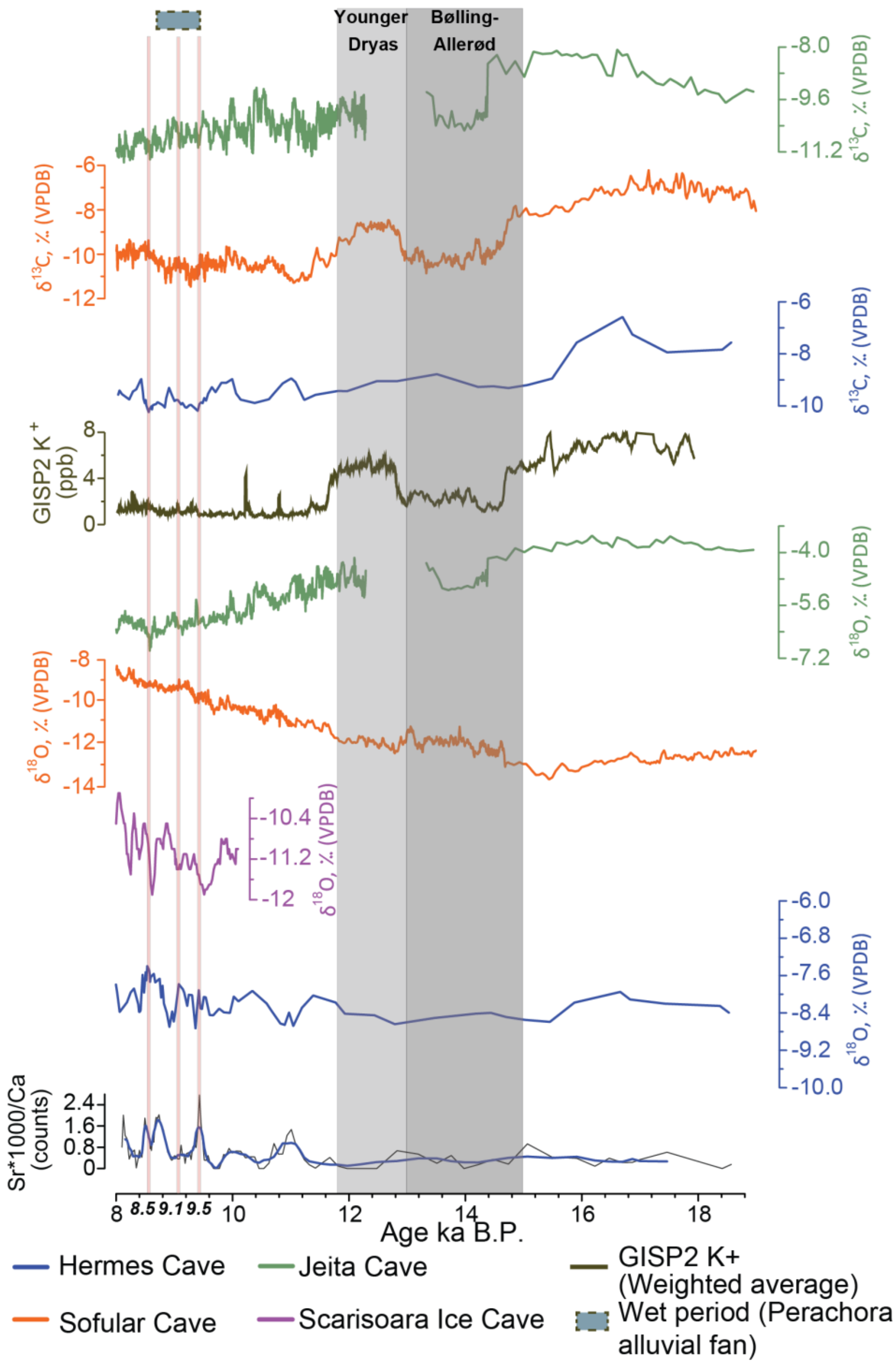

Figure 8. Comparison of ZCG1 post LGM part with other records from the broader area (see text for details).

The μ-XRF results exhibit high variation on the Sr/Ca ratio which in combination with the stable isotopes can be used as indicators of seasonal environmental changes. The curve presents a prominent peak at 123-122 ka that correlates with lower values in carbon record and a period of high oxygen values. The Sr and carbon isotope values suggest wet and warm summers that enhanced soil production in the area but without such warm values or high rainfall amounts that oxygen isotopes were significantly decreased. Again, an increase local, high $\delta^{18}O$, moisture sources at this time would also help to explain the peristing high oxygen isotope values. The period from 115 ka until the halt in stalagmite growth implies different climatic condition relative to the older part of the stalagmite. In this younger period there are four prominent positive peaks in the curve at ca 114, 112.5, 107and 105 ka that correlate with higher peaks in oxygen and lower peaks in carbon record. This implies that the area was experiencing more precipitation during summer months, but the soil production was low since there is already a transition towards the last glacial period and mean temperature is decreasing. Finally, in the early Holocene section of the stalagmite, we observe four positive peaks in the Sr/Ca record centered 9.5, and 8.5 ka that corelate with negative peaks in the carbon record and higher values at the oxygen record that suggest wet conditions during these periods that favored soil formation (Fig.8).

Consequently, for the early Holocene, we suggest that easterly winds driven by a strengthened Siberian High resulted in moisture pick-up from the warm surface waters of the Aegean Sea and subsequent increased precipitation in mainland Greece.

5.2 Climatic impact on sediment delivery

Recent results from the IODP Expedition 381 into the Corinth Gulf (Shillington et al., 2019) show a profound variability in sediment accumulation rates in response to climate changes during the Quaternary. In particular, relatively low sedimentation rates (0.3-0.7 mm/yr) are infered for the last interglacial period (i.e. MIS 5) in contrast to the higher sedimentation rates that characterize the last glacial (~2.5 mm/yr) and the Holocene (2.5-3 mm/yr). McNeill et al (2019) argue that the observed variability in sediment flux is due to changes in the type of vegetation cover, while the increased sedimentation rates during the Holocene are attributed to human deforestation in the area from 6000 yr onward. Our results from the lower part of the ZCG1 stalagmite that suggest high soil productivity indicative of an extended vegetation coverage in the area during the oldest parts of MIS 5. During this period, erosion rates were likely depleted by vegetation and fluvial network delivered less sediment into the Gulf of Corinth. Towards the demise of peak (penultimate) interglacial conditions, our data show a decline in soil productivity inferred by higher values of $^{13}\delta C$. This is consistent with the results from other studies that imply the development of a weak vegetation cover in the Balkan peninsula (e.g. Tzedakis et al., 2004). Although the stalagmite growth halts during the last glacial period possibly due to shortage of water infiltrating Hermes Cave as a result of the expansion of high altitude small glaciers, at lower elevations there was probably an abundance of meltwater feeding the fluvial network. This combination of weak vegetation cover and high-water supply during the last glacial period drove the high sedimentation rates observed in the Gulf of Corinth (McNeill et al., 2019). The younger part of the stalagmite (post the growth hiatus) suggests a warmer and wetter period. During this period the vegetation didn't recover from the last glacial period since most of the soil was eroded away, thus enabling only low/open vegetation to grow. This, in combination with the icecap/glacier melting resulted in higher erosion rates on the flanks of the Corinth Rift leading to increased sediment accumulation into the gulf during the onset of Holocene.

6. Conclusions

This study contributes to the paleoclimatic reconstruction of the Eastern Mediterranean over the Quaternary using a speleothem (ZCG1) from the Hermes Cave, which is located at the southern flanks of the Corinth Rift, central Greece. Our particular findings are the following:

- The ZCG1 formation started at ~127 ka marking the establishment of climatic conditions that favored the speleothem deposition. This period coincides with the beginning of the maximum interglacial conditions which enabled the high growth rates observed in stalagmites in Europe.
- We show that a low soil productivity period prevailed in the area from 122 to ca 117 ka B.P. implying overall dryer climatic conditions. This is in disagreenment to the wetter climatic conditions observed in central Europe during the so called ‘last Interglacial optimum’. Dry conditions settle in the area later on until the begining of MIS4, when the stalagmite stops growing at ca 105 ka B.P.
- The growth hiatus of ZCG1 from 105 to 23 ka B.P. occurred most probably due to low amounts of water infiltrating into the cave since the area was covered by small glaciers that also expanded during the glacial period.

- Our record exhibits higher temporal resolution towards the onset of the Holocene due to higher growth rate that is attributed to increased soil productivity under warm and wet climatic conditions.
- ZCG1 record presents similaraties with other records in the broader area of the Eastern Mediterranean. Specifically, during the Bølling-Allerød (BA) and Younger Dryas (YD) our data suggest enhanced soil productivity linked to post-glacial forest expansion during the warm BA and increased precipitation delivered by strengthened westerlies due to southward displacement of the polar front during the YD. Our data show a clear differentiation of climatic conditions during the YD between SE Europe and the Eastern Mediterranean region. During the Early Holocene three warm and wet periods at 8.5, 9.4 ka and 10.1 ka respectively mark the overall warming trend. These warm periods resulted when cold air outbursts associated with a strengthened Siberian High were not strong enough to generate cold conditions over mainland Greece, but these clockwise mowing winds likely picked-up moisture from the Aegean Sea and led to higher than usual precipitation over the area.
- Our record shows high variability in soil productivity and precipitation. The combining effect of these two parameters is the controlling factor on catchment averaged erosion rates with implications to sediment delivery into the Gulf of Corinth.

7. Acknowledgements

The authors would like to express their gratitude to cavers Yorgos Sotiriadis, Charikleia Gkarlaouni, Christina Gkarlaouni and Nikolaos Kortimanitsis for their invaluable help during our visit in the Hermes Cave. Ephorate of Palaeoanthropology and Speleology of the Hellenic Ministry of Culture is thanked for granting permission to work inside the cave

(ΥΠΠΟΑ/ΓΔΑΠΚ/ΕΠΣ/ΤΑΕΜΓΠ/87570/59775/1006/40). RG acknowledges the award of the VISTA Professorship from the Norwegian Academy of Science and Letters. SP and some of the analytical work were also funded by the VISTA Professorship award. AP was supported by the Romanian Ministry of Education and Research, CNCS - UEFISCDI, project number PN-III-P4-ID-PCE-2020-2723, within PNCDI III. This work was inspired by the conversations we had with late Prof. Patience Cowie, a great colleague and mentor.

8. References

Bar-Matthews, M., Ayalon, A., and Kaufman, A. (2000). Timing and hydrological conditions of Sapropel events in the Eastern Mediterranean, as evident from speleothems, Soreq cave, Israel. *Chemical Geology* 169(1-2), 145-156. doi: Doi 10.1016/S0009-2541(99)00232-6.

Bourdon, B. (2003). Introduction to U-series Geochemistry. *Reviews in Mineralogy and Geochemistry* 52(1), 1-21. doi: 10.2113/0520001.

Boyd, M. (2015). *Speleothems from Warm Climates : Holocene Records from the Caribbean and Mediterranean Regions.* Doctoral thesis, comprehensive summary, Department of Physical Geography, Stockholm University.

Cheng, H., Sinha, A., Verheyden, S., Nader, F.H., Li, X.L., Zhang, P.Z., et al. (2015). The climate variability in northern Levant over the past 20,000 years. *Geophysical Research Letters* 42(20), 8641-8650. doi: 10.1002/2015gl065397.

Constantin, S., Bojar, A.-V., Lauritzen, S.-E., and Lundberg, J.: Holocene and Late Pleistocene climate in the sub-Mediterranean continental environment: A speleothem record from Poleva Cave (Southern Carpathians, Romania), Palaeogeography, Palaeoclimatology, Palaeoecology, 243, 322–338, https://doi.org/10.1016/j.palaeo.2006.08.001, 2007.

Coplen, T.B., Brand, W.A., Gehre, M., Groning, M., Meijer, H.A., Toman, B., et al. (2006). New guidelines for delta13C measurements. *Anal Chem* 78(7), 2439-2441. doi: 10.1021/ac052027c.

Cohen, J., Saito, K., and Entekhabi, D.: The role of the Siberian high in northern hemisphere climate variability, Geophys. Res. Lett., 28, 299–302, https://doi.org/10.1029/2000GL011927, 2001

Croudace, I.W., Rindby, A., and Rothwell, R.G. (2006). ITRAX: description and evaluation of a new multi-function X-ray core scanner. *Geological Society, London, Special Publications* 267(1)**,** 51-63. doi: 10.1144/gsl.Sp.2006.267.01.04.

Dansgaard, W. (1964). Stable isotopes in precipitation. *Tellus* 16(4), 436-468. doi: 10.1111/j.2153-3490.1964.tb00181.x.

Demény, A., Kern, Z., Czuppon, G., Németh, A., Leél-Őssy, S., Siklósy, Z., et al. (2017). Stable isotope compositions of speleothems from the last interglacial – Spatial patterns of climate fluctuations in Europe. *Quaternary Science Reviews* 161**,** 68-80. doi: 10.1016/j.quascirev.2017.02.012.

Drysdale, R.N., Hellstrom, J.C., Zanchetta, G., Fallick, A.E., Sanchez Goni, M.F., Couchoud, I., et al. (2009). Evidence for obliquity forcing of glacial Termination II. *Science* 325(5947)**,** 1527-1531. doi: 10.1126/science.1170371.

Fairchild, I.J., and Baker, A. (2012). *Speleothem science : from process to past environments / Ian J. Fairchild and Andy Baker ; with contributions from Asfawossen Asrat ... [et al.].* Chichester, U.K: Wiley Blackwell.

Fairchild, I.J., and Treble, P.C. (2009). Trace elements in speleothems as recorders of environmental change. *Quaternary Science Reviews* 28(5-6)**,** 449-468. doi: 10.1016/j.quascirev.2008.11.007.

Feidas, H., Noulopoulou, C., Makrogiannis, T., and Bora-Senta, E. (2007). Trend analysis of precipitation time series in Greece and their relationship with circulation using surface and satellite data: 1955-2001. *Theoretical and Applied Climatology* 87(1-4)**,** 155-177. doi: 10.1007/s00704-006-0200-5.

Feurdean, A., Perşoiu, A., Tanţău, I., Stevens, T., Magyari, E. K., Onac, B. P., Marković, S., Andrič, M., Connor, S., Fărcaş, S., Gałka, M., Gaudeny, T., Hoek, W., Kolaczek, P., Kuneš, P., Lamentowicz, M., Marinova, E., Michczyńska, D. J., Perşoiu, I., Płóciennik, M., Słowiński, M., Stancikaite, M., Sumegi, P., Svensson, A., Tămaş, T., Timar, A., Tonkov, S., Toth, M., Veski, S., Willis, K. J., and Zernitskaya, V.: Climate variability and associated vegetation response throughout Central and Eastern Europe (CEE) between 60 and 8 ka, Quaternary Science Reviews, 106, 206–224, https://doi.org/10.1016/j.quascirev.2014.06.003, 2014.

Finné, M., Bar-Matthews, M., Holmgren, K., Sundqvist, H.S., Liakopoulos, I., and Zhang, Q. (2014). Speleothem evidence for late Holocene climate variability and floods in Southern Greece. *Quaternary Research* 81(2)**,** 213-227. doi: 10.1016/j.yqres.2013.12.009.

Finné, M., Kylander, M., Boyd, M., Sundqvist, H., and Löwemark, L. (2015). Can XRF scanning of speleothems be used as a non-destructive method to identify paleoflood events in caves? *International Journal of Speleology* 44(1)**,** 17-23. doi: 10.5038/1827-806x.44.1.2.

Fleitmann, D., Cheng, H., Badertscher, S., Edwards, R.L., Mudelsee, M., Göktürk, O.M., et al. (2009). Timing and climatic impact of Greenland interstadials recorded in stalagmites from northern Turkey. *Geophysical Research Letters* 36(19)**,** L19707. doi: 10.1029/2009gl040050.

Friedman, I., O'Neil, J., and Cebula, G. (1982). Two New Carbonate Stable-Isotope Standards. *Geostandards and Geoanalytical Research* 6(1), 11-12. doi: 10.1111/j.1751-908X.1982.tb00340.x.

Gawthorpe, R.L., Leeder, M.R., Kranis, H., Skourtsos, E., Andrews, J.E., Henstra, G.A., et al. (2018). Tectono-sedimentary evolution of the Plio-Pleistocene Corinth rift, Greece. *Basin Research* 30(3)**,** 448-479. doi: 10.1111/bre.12260.

Genty, D., Baker, A., and Vokal, B. (2001). Intra- and inter-annual growth rate of modern stalagmites. *Chemical Geology* 176(1-4), 191-212. doi: 10.1016/s0009-2541(00)00399-5.

Genty, D., Verheyden, S., and Wainer, K. (2013). Speleothem records over the last interglacial. *PAGES news* 21(1)**,** 24-25. doi: 10.22498/pages.21.1.24.

Gogou, A., Triantaphyllou, M., Xoplaki, E., Izdebski, A., Parinos, C., Dimiza, M., et al. (2016). Climate variability and socio-environmental changes in the northern Aegean (NE Mediterranean) during the last 1500 years. *Quaternary Science Reviews* 136**,** 209-228. doi: 10.1016/j.quascirev.2016.01.009.

Govin, A., Capron, E., Tzedakis, P.C., Verheyden, S., Ghaleb, B., Hillaire-Marcel, C., et al. (2015). Sequence of events from the onset to the demise of the Last Interglacial: Evaluating strengths and limitations of chronologies used in climatic archives. *Quaternary Science Reviews* 129**,** 1-36. doi: 10.1016/j.quascirev.2015.09.018.

Hendy, C.H. (1971). The isotopic geochemistry of speleothems—I. The calculation of the effects of different modes of formation on the isotopic composition of speleothems and their applicability as palaeoclimatic indicators. *Geochimica et Cosmochimica Acta* 35(8), 801-824. doi: 10.1016/0016-7037(71)90127-x.

Hercman, H., and Pawlak, J. (2012). MOD-AGE: An age-depth model construction algorithm. *Quaternary Geochronology* 12, 1-10. doi: Doi 10.1016/J.Quageo.2012.05.003.

Hut, G. (1987). "Consultants' group meeting on stable isotope reference samples for geochemical and hydrological investigations", in: *Consultants' group meeting on stable isotope reference samples for geochemical and hydrological investigations*).

Jones, T.D., Lawson, I.T., Reed, J.M., Wilson, G.P., Leng, M.J., Gierga, M., et al. (2012). Diatom-inferred late Pleistocene and Holocene palaeolimnological changes in the Ioannina basin, northwest Greece. *Journal of Paleolimnology* 49(2), 185-204. doi: 10.1007/s10933-012-9654-x.

Katrantsiotis, C., Norström, E., Smittenberg, R.H., Finne, M., Weiberg, E., Hättestrand, M., et al. (2019). Climate changes in the Eastern Mediterranean over the last 5000 years and their links to the high-latitude atmospheric patterns and Asian monsoons. *Global and Planetary Change* 175, 36-51. doi: 10.1016/j.gloplacha.2019.02.001.

Kern, Z., Demény, A., Perşoiu, A., and Hatvani, I.G. (2019). Speleothem Records from the Eastern Part of Europe and Turkey—Discussion on Stable Oxygen and Carbon Isotopes. *Quaternary* 2(3). doi: 10.3390/quat2030031.

Kluge, T., Münster, T.S., Frank, N., Eiche, E., Mertz-Kraus, R., Scholz, D., et al. doi: 10.5194/cp-2020-47.

Koukousioura, O., Triantaphyllou, M.V., Dimiza, M.D., Pavlopoulos, K., Syrides, G., and Vouvalidis, K. (2012). Benthic foraminiferal evidence and paleoenvironmental evolution of Holocene coastal plains in the Aegean Sea (Greece). *Quaternary International* 261**,** 105-117. doi: Doi 10.1016/J.Quaint.2011.07.004.

Kouli, K., Gogou, A., Bouloubassi, I., Triantaphyllou, M.V., Ioakim, C., Katsouras, G., et al. (2012). Late postglacial paleoenvironmental change in the northeastern Mediterranean region: Combined palynological and molecular biomarker evidence. *Quaternary International* 261**,** 118-127. doi: 10.1016/j.quaint.2011.10.036.

Lane, C. S., Brauer, A., Blockley, S. P. E., and Dulski, P.: Volcanic ash reveals time-transgressive abrupt climate change during the Younger Dryas, Geology, 41, 1251–1254, https://doi.org/10.1130/G34867.1, 2013.

Leontaritis, A.D., Kouli, K., and Pavlopoulos, K. (2020). The glacial history of Greece: a comprehensive review. *Mediterranean Geoscience Reviews*. doi: 10.1007/s42990-020-00021-w.

Lespez, L., Glais, A., Lopez-Saez, J.-A., Le Drezen, Y., Tsirtsoni, Z., Davidson, R., et al. (2017). Middle Holocene rapid environmental changes and human adaptation in Greece. *Quaternary Research* 85(02)**,** 227-244. doi: 10.1016/j.yqres.2016.02.002.

Lionello, P., Malanotte-Rizzoli, P., Boscolo, R., Alpert, P., Artale, V., Li, L., et al. (2006). "The Mediterranean climate: An overview of the main characteristics and issues," in *Mediterranean,* eds. P. Lionello, P. Malanotte-Rizzoli & R. Boscolo. Elsevier), 1-26.

Ludwig, K.R. (2003). Isoplot 3.00: A geochronological toolkit for Microsoft Excel. *Berkeley Geochronology Center Special Publication* 4**,** 70.

Mamara, A., Anadranistakis, M., Argiriou, A.A., Szentimrey, T., Kovacs, T., Bezes, A., et al. (2017). High resolution air temperature climatology for Greece for the period 1971-2000. *Meteorological Applications* 24(2)**,** 191-205. doi: 10.1002/met.1617.

Marino, G., Rohling, E.J., Sangiorgi, F., Hayes, A., Casford, J.L., Lotter, A.F., et al. (2009). Early and middle Holocene in the Aegean Sea: interplay between high and low latitude climate variability. *Quaternary Science Reviews* 28(27-28)**,** 3246-3262. doi: 10.1016/j.quascirev.2009.08.011.

Mayewski, P.A., Meeker, L.D., Twickler, M.S., Whitlow, S., Yang, Q., Lyons, W.B., et al. (1997). Major features and forcing of high-latitude northern hemisphere atmospheric circulation using a 110,000-year-long glaciochemical series. *Journal of Geophysical Research: Oceans* 102(C12)**,** 26345-26366. doi: 10.1029/96jc03365.

Mayewski, P.A., Rohling, E.E., Curt Stager, J., Karlén, W., Maasch, K.A., David Meeker, L., et al. (2004). Holocene climate variability. *Quaternary Research* 62(3)**,** 243-255. doi: 10.1016/j.yqres.2004.07.001.

McDermott, F. (2004). Palaeo-climate reconstruction from stable isotope variations in speleothems: a review. *Quaternary Science Reviews* 23(7-8), 901-918. doi: 10.1016/j.quascirev.2003.06.021.

McNeill, L.C., Shillington, D.J., Carter, G.D.O., Everest, J.D., Gawthorpe, R.L., Miller, C., et al. (2019). High-resolution record reveals climate-driven environmental and sedimentary changes in an active rift. *Scientific Reports* 9(1). doi: 10.1038/s41598-019-40022-w.

Milner, A.M., Müller, U.C., Roucoux, K.H., Collier, R.E.L., Pross, J., Kalaitzidis, S., et al. (2013). Environmental variability during the Last Interglacial: a new high-resolution pollen record from Tenaghi Philippon, Greece. *Journal of Quaternary Science* 28(2)**,** 113-117. doi: 10.1002/jqs.2617.

Nehme, C., Kluge, T., Verheyden, S., Nader, F., Charalambidou, I., Weissbach, T., et al. (2020). Speleothem record from Pentadactylos cave (Cyprus): new insights into climatic variations during MIS 6 and MIS 5 in the Eastern Mediterranean. *Quaternary Science Reviews* 250. doi: 10.1016/j.quascirev.2020.106663.

Nehme, C., Verheyden, S., Breitenbach, S.F.M., Gillikin, D.P., Verheyden, A., Cheng, H., et al. (2018). Climate dynamics during the penultimate glacial period recorded in a speleothem from Kanaan Cave, Lebanon (central Levant). *Quaternary Research* 90(1)**,** 10-25. doi: 10.1017/qua.2018.18.

Nehme, C., Verheyden, S., Noble, S.R., Farrant, A.R., Sahy, D., Hellstrom, J., et al. (2015). Reconstruction of MIS 5 climate in the central Levant using a stalagmite from Kanaan Cave, Lebanon. *Climate of the Past* 11(12)**,** 1785-1799. doi: 10.5194/cp-11-1785-2015.

Peckover, E.N., Andrews, J.E., Leeder, M.R., Rowe, P.J., Marca, A., Sahy, D., et al. (2019). Coupled stalagmite – Alluvial fan response to the 8.2 ka event and early Holocene palaeoclimate change in Greece. *Palaeogeography, Palaeoclimatology, Palaeoecology*. doi: 10.1016/j.palaeo.2019.109252.

Pennos, C., Pechlivanidou, S., Aidona, E., Bourliva, A., Lauritzen, S.-E., Scholger, R., et al. (2021). Decoding short-term climatic variations from cave sediments over the Mid-Holocene: Implications for human occupation in the Katarraktes Cave System, Northern Greece. *Zeitschrift für Geomorphologie*. doi: 10.1127/zfg/2021/0680.

Perșoiu, A., Onac, B. P., Wynn, J. G., Blaauw, M., Ionita, M., and Hansson, M. (2017). Holocene winter climate variability in Central and Eastern Europe. Scientific Reports 7, 1196. doi:10.1038/s41598-017-01397-w.

Perşoiu, A., Ionita, M., and Weiss, H. (2019). Atmospheric blocking induced by the strengthened Siberian High led to drying in west Asia during the 4.2 ka BP event – a hypothesis. Clim. Past 15, 781–793. doi:10.5194/cp-15-781-2019.

Petrocheilou, A. (1972). Cave of Herme's or Cave of Pan or Cave of Apollo or Killini's hole (in Greek). *Annals of Hellenic Speleological Society* 11(5-6)**,** 8.

Philandras, C.M., Nastos, P.T., Kapsomenakis, J., Douvis, K.C., Tselioudis, G., and Zerefos, C.S. (2011). Long term precipitation trends and variability within the Mediterranean region. Natural Hazards and Earth System Sciences 11(12), 3235-3250. doi: 10.5194/nhess-11-3235-2011.

Portman, C., Andrews, J.E., Rowe, P.J., Leeder, M.R., and Hoogewerff, J. (2005). Submarine-spring controlled calcification and growth of large Rivularia bioherms, Late Pleistocene (MIS 5e), Gulf of Corinth, Greece. *Sedimentology* 52(3), 441-465. doi: 10.1111/j.1365-3091.2005.00704.x.

Psomiadis, D., Dotsika, E., Albanakis, K., Ghaleb, B., and Hillaire-Marcel, C. (2018). Speleothem record of climatic changes in the northern Aegean region (Greece) from the Bronze Age to the collapse of the Roman Empire. *Palaeogeography, Palaeoclimatology, Palaeoecology* 489**,** 272-283. doi: 10.1016/j.palaeo.2017.10.021.

Psomiadis, D., Dotsika, E., Zisi, N., Pennos, C., Pechlivanidou, S., Albanakis, K., et al. (2009). Geoarchaeological study of Katarraktes cave system (Macedonia, Greece): isotopic evidence for environmental alterations. *Geomorphologie-Relief Processus Environnement* 15(4)**,** 229-240. doi: 10.4000/geomorphologie.7694.

Regattieri, E., Isola, I., Giovanni Zanchetta, Andrea Tognarelli, John C. Hellstrom, Russell N. Drysdale, et al. (2020). Middle - Holocene climate variability from a stalagmite from Alilica Cave (Southern Balkans). *Alpine and Mediterranean Quaternary* 1(32). doi: 10.26382/AMQ.2019.02.

Regattieri, E., Zanchetta, G., Isola, I., Bajo, P., Boschi, C., Perchiazzi, N., et al. (2018). A MIS 9/MIS 8 speleothem record of hydrological variability from Macedonia (F.Y.R.O.M.). *Global and Planetary Change*. doi: 10.1016/j.gloplacha.2018.01.003.

Remoundaki, E., Bourliva, A., Kokkalis, P., Mamouri, R.E., Papayannis, A., Grigoratos, T., et al. (2011). PM10 composition during an intense Saharan dust transport event over Athens (Greece). Sci Total Environ 409(20), 4361-4372. doi: 10.1016/j.scitotenv.2011.06.026

Rohling, E.J., Marino, G., and Grant, K.M. (2015). Mediterranean climate and oceanography, and the periodic development of anoxic events (sapropels). *Earth-Science Reviews* 143**,** 62-97. doi: 10.1016/j.earscirev.2015.01.008.

Rohling, E.J., Marino, G., Grant, K.M., Mayewski, P.A., and Weninger, B. (2019). A model for archaeologically relevant Holocene climate impacts in the Aegean-Levantine region (easternmost Mediterranean). *Quaternary Science Reviews* 208**,** 38-53. doi: 10.1016/j.quascirev.2019.02.009.

Shillington, D., McNeill, L., Carter, G., and and the Expedition 381 Participants. (2019). Expedition 381 Preliminary Report: Corinth Active Rift Development. *International Ocean Discovery Program*. doi: https://doi.org/10.14379/iodp.pr.381.2019.

Skourtsos, E., Kranis, H., Zambetakis-Lekkas, A., Gawthorpe, R., and Leeder, M. (2017). Alpine Basement Outcrops at Northern Peloponnesus: Implications for the Early Stages in the Evolution of the Corinth Rift. *Bulletin of the Geological Society of Greece* 50(1). doi: 10.12681/bgsg.11714.

Stichler, W. (1995). "Interlaboratory comparison of new materials for carbon and oxygen isotope ratio measurements". (International Atomic Energy Agency (IAEA)).

Stuut, J.-B., Smalley, I., and O'Hara-Dhand, K. (2009). Aeolian dust in Europe: African sources and European deposits. *Quaternary International* 198(1-2), 234-245. doi: 10.1016/j.quaint.2008.10.007.

Styllas, M.N., and Ghilardi, M. (2017). Early- to mid-Holocene paleohydrology in northeast Mediterranean: The detrital record of Aliakmon River in Loudias Lake, Greece. *The Holocene* 27(10)**,** 1487-1498. doi: 10.1177/0959683617693905.

Styllas, M.N., Schimmelpfennig, I., Benedetti, L., Ghilardi, M., Aumaître, G., Bourlès, D., et al. (2018). Late-glacial and Holocene history of the northeast Mediterranean mountains - New insights from in situ -produced 36 Cl - based cosmic ray exposure dating of paleo-glacier deposits on Mount Olympus, Greece. *Quaternary Science Reviews* 193**,** 244-265. doi: 10.1016/j.quascirev.2018.06.020.

Styllas, M.N., Schimmelpfennig, I., Ghilardi, M., and Benedetti, L. (2015). Geomorphologic and paleoclimatic evidence of Holocene glaciation on Mount Olympus, Greece. *The Holocene*. doi: 10.1177/0959683615618259

Triantaphyllou, M.V., Gogou, A., Dimiza, M.D., Kostopoulou, S., Parinos, C., Roussakis, G., et al. (2015). Holocene Climatic Optimum centennial-scale paleoceanography in the NE Aegean (Mediterranean Sea). *Geo-Marine Letters* 36(1)**,** 51-66. doi: 10.1007/s00367-015-0426-2.

Triantaphyllou, M.V., Ziveri, P., Gogou, A., Marino, G., Lykousis, V., Bouloubassi, I., et al. (2009). Late Glacial–Holocene climate variability at the south-eastern margin of the Aegean Sea. *Marine Geology* 266(1-4)**,** 182-197. doi: 10.1016/j.margeo.2009.08.005.

Tzedakis, P.C. (2010). The MIS 11-MIS 1 analogy, southern European vegetation, atmospheric methane and the 'early anthropogenic hypothesis'. *Climate of the Past* 6(2)**,** 131-144. doi: 10.5194/cp-6-131-2010.

Tzedakis, P.C., Drysdale, R.N., Margari, V., Skinner, L.C., Menviel, L., Rhodes, R.H., et al. (2018). Enhanced climate instability in the North Atlantic and southern Europe during the Last Interglacial. Nat Commun 9(1), 4235. doi: 10.1038/s41467-018-06683-3.

Tzedakis, P.C., Frogley, M.R., and Heaton, T.H.E. (2002). Duration of Last Interglacial Conditions in Northwestern Greece. *Quaternary Research* 58(1)**,** 53-55. doi: 10.1006/qres.2002.2328.

Tzedakis, P.C., Frogley, M.R., Lawson, I.T., Preece, R.C., Cacho, I., and de Abreu, L. (2004). Ecological thresholds and patterns of millennial-scale climate variability: The response of vegetation in Greece during the last glacial period. *Geology* 32(2)**,** 109-112. doi: 10.1130/G20118.1.

Tzedakis, P.C., Hooghiemstra, H., and Pälike, H. (2006). The last 1.35 million years at Tenaghi Philippon: revised chronostratigraphy and long-term vegetation trends. *Quaternary Science Reviews* 25(23-24)**,** 3416-3430. doi: 10.1016/j.quascirev.2006.09.002.

Wong, C.I., Banner, J.L., and Musgrove, M. (2011). Seasonal dripwater Mg/Ca and Sr/Ca variations driven by cave ventilation: Implications for and modeling of speleothem paleoclimate records. *Geochimica Et Cosmochimica Acta* 75(12)**,** 3514-3529. doi: 10.1016/j.gca.2011.03.025.

Xoplaki, E., Gonzalez-Rouco, J.F., Luterbacher, J., and Wanner, H. (2004). Wet season Mediterranean precipitation variability: influence of large-scale dynamics and trends. *Climate Dynamics* 23(1)**,** 63-78. doi: 10.1007/s00382-004-0422-0.

Xoplaki, E., Luterbacher, J., Burkard, R., Patrikas, I., and Maheras, P. (2000). Connection between the large-scale 500 hPa geopotential height fields and precipitation over Greece during wintertime. *Climate Research* 14(2)**,** 129-146. doi: DOI 10.3354/cr014129.

Zerefos, C., Repapis, C., Giannakopoulos, C., Kapsomenakis, J., Papanikolaou, D., Papanikolaou, M., et al. (2011). The climate of the Eastern Mediterranean and Greece: past, present and future. *The Environmental, Economic and Social Impacts of Climate Change in Greece***,** 50-58.